Electronic Supplementary Information

From zero-dimensional metallomacrocycle to three-dimensional metal–organic frameworks mediated by solvent polarity: Near-white light emissions and gas adsorption properties

Jia-Ling Yin,[a] Qing-Qing Yan,[a] Yu-Xin Liu[b] and Guo-Ping Yong*[a]

[a] Department of Chemistry, University of Science and Technology of China, Hefei 230026, P. R. China. E-mail: gpyong@ustc.edu.cn
[b] Technology Center of Hefei Customs, and Anhui Province Key Laboratory of Analysis and Detection for Food Safety, Hefei, 230022, P. R. China.

Table S1 Selected bond distances (Å) and angles (º) for **1**, **2** and **6**.[a]

1		**2**		**6**	
Mn(1)-O(1)	2.103(4)	Mn(1)-O(1)	2.106(4)	Zn(1)-O(1)	1.915(2)
Mn(1)-O(3)	2.103(4)	Mn(1)-O(3)#4	2.108(5)	Zn(1)-O(6)#3	1.937(2)
Mn(1)-O(5)	2.196(4)	Mn(1)-N(1)	2.332(5)	Zn(1)-O(9)	2.023(3)
Mn(1)-O(6)	2.162(4)	Mn(1)-N(2)#3	2.244(6)	Zn(1)-O(10)	1.964(3)
Mn(1)-N(1)	2.351(5)	Mn(1)-N(3)#4	2.349(6)	Zn(2)-O(4)#2	2.000(5)
Mn(1)-N(2)	2.373(5)	Mn(1)-N(4)#2	2.224(6)	Zn(2)-O(7)	1.908(3)
Mn(2)-O(7)	2.110(4)	O(1)-Mn(1)-O(3)#4	178.08(19)	Zn(2)-O(11)	1.920(4)
Mn(2)-O(9)	2.114(4)	O(1)-Mn(1)-N(1)	74.58(19)	O(1)-Zn(1)-O(6)#3	125.33(10)
Mn(2)-O(11)	2.138(4)	O(1)-Mn(1)-N(2)#3	91.55(19)	O(1)-Zn(1)-O(9)	95.97(11)
Mn(2)-O(12)	2.175(4)	O(1)-Mn(1)-N(3)#4	104.66(19)	O(1)-Zn(1)-O(10)	109.94(12)
Mn(2)-N(3)	2.435(5)	O(1)-Mn(1)-N(4)#2	89.22(19)	O(6)#3-Zn(1)-O(9)	103.06(10)
Mn(2)-N(4)	2.357(4)	O(3)#4-Mn(1)-N(1)	103.6(2)	O(6)#3-Zn(1)-O(10)	115.13(11)
O(1)-Mn(1)-O(3)	167.30(16)	O(3)#4-Mn(1)-N(2)#3	89.31(19)	O(9)-Zn(1)-O(10)	102.07(11)
O(1)-Mn(1)-O(5)	82.27(14)	O(3)#4-Mn(1)-N(3)#4	74.30(18)	O(4)#2-Zn(2)-O(7)	140.9(2)
O(1)-Mn(1)-O(6)	95.12(18)	O(3)#4-Mn(1)-N(4)#2	92.6(2)	O(4)#2-Zn(2)-O(11)	89.9(2)
O(1)-Mn(1)-N(1)	73.44(15)	N(1)-Mn(1)-N(2)#3	100.1(2)	O(7)-Zn(2)-O(11)	102.4(2)
O(1)-Mn(1)-N(2)	110.67(18)	N(1)-Mn(1)-N(3)#4	79.0(2)		
O(3)-Mn(1)-O(5)	85.07(15)	N(1)-Mn(1)-N(4)#2	163.4(2)		
O(3)-Mn(1)-O(6)	85.68(15)	N(2)#3-Mn(1)-N(3)#4	162.7(2)		
O(3)-Mn(1)-N(1)	119.26(16)	N(2)#3-Mn(1)-N(4)#2	83.8(2)		

O(3)-Mn(1)-N(2)	72.85(15)	N(3)#4-Mn(1)-N(4)#2	102.0(2)
O(5)-Mn(1)-O(6)	88.87(15)		
O(5)-Mn(1)-N(1)	155.42(15)		
O(5)-Mn(1)-N(2)	110.28(17)		
O(6)-Mn(1)-N(1)	89.53(16)		
O(6)-Mn(1)-N(2)	149.28(16)		
N(1)-Mn(1)-N(2)	82.47(17)		
O(7)-Mn(2)-O(9)	172.33(16)		
O(7)-Mn(2)-O(11)	84.97(15)		
O(7)-Mn(2)-O(12)	85.86(16)		
O(7)-Mn(2)-N(3)	72.75(15)		
O(7)-Mn(2)-N(4)	112.40(16)		
O(9)-Mn(2)-O(11)	90.96(16)		
O(9)-Mn(2)-O(12)	88.25(15)		
O(9)-Mn(2)-N(3)	112.82(16)		
O(9)-Mn(2)-N(4)	74.38(14)		
O(11)-Mn(2)-	97.82(17)		
O(12)	152.87(15)		
O(11)-Mn(2)-N(3)	94.85(16)		
O(11)-Mn(2)-N(4)	95.85(17)		
O(12)-Mn(2)-N(3)	158.65(15)		
O(12)-Mn(2)-N(4)	80.07(16)		
N(3)-Mn(2)-N(4)			

[a] Symmetry code for **2**: #2= -x, y+1/2, -z+1/2, #3=-x, -y, -z, #4=x, -y-1/2, z-1/2; symmetry code for **6**: #2= -x, y+1/2, -z+1/2, #3= -x, -y, -z.

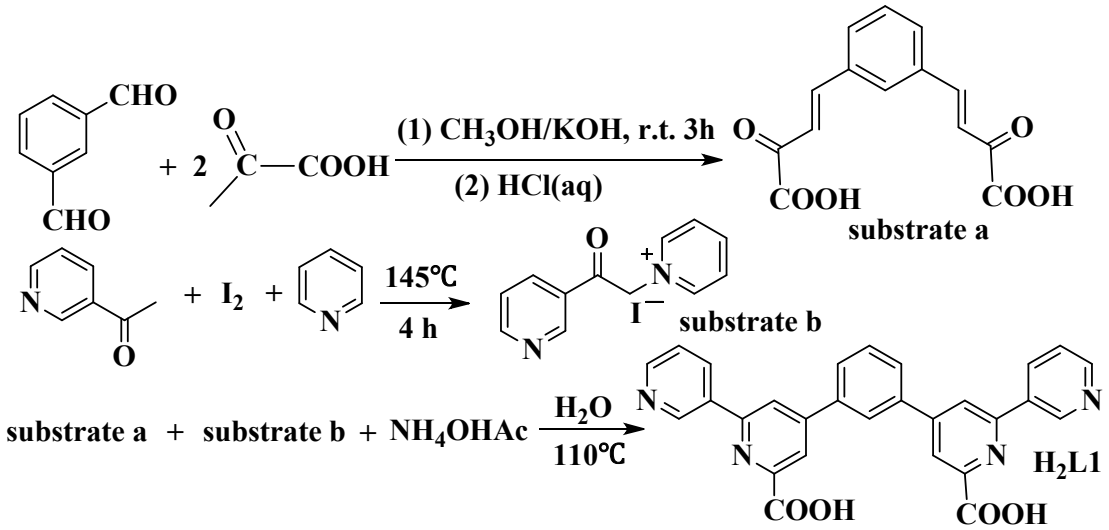

Scheme S1 The synthesis procedure for H_2L1 ligand.

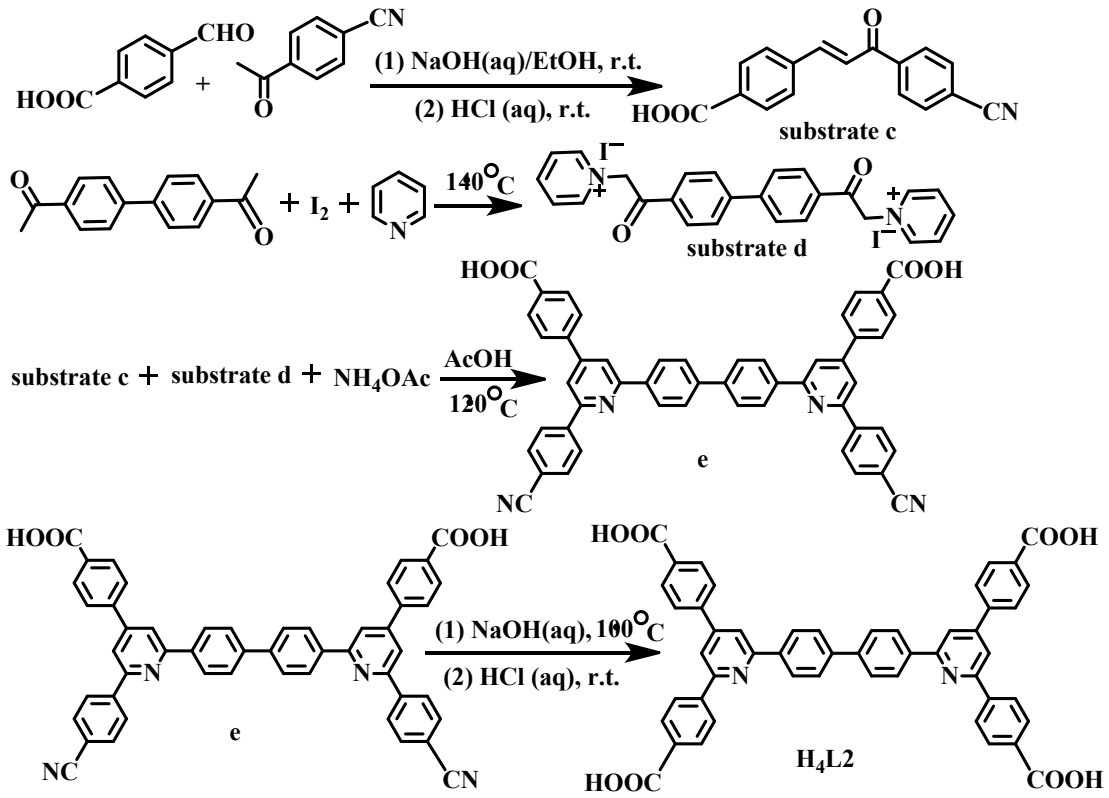

Scheme S2 The synthesis procedure for H_4L2 ligand.

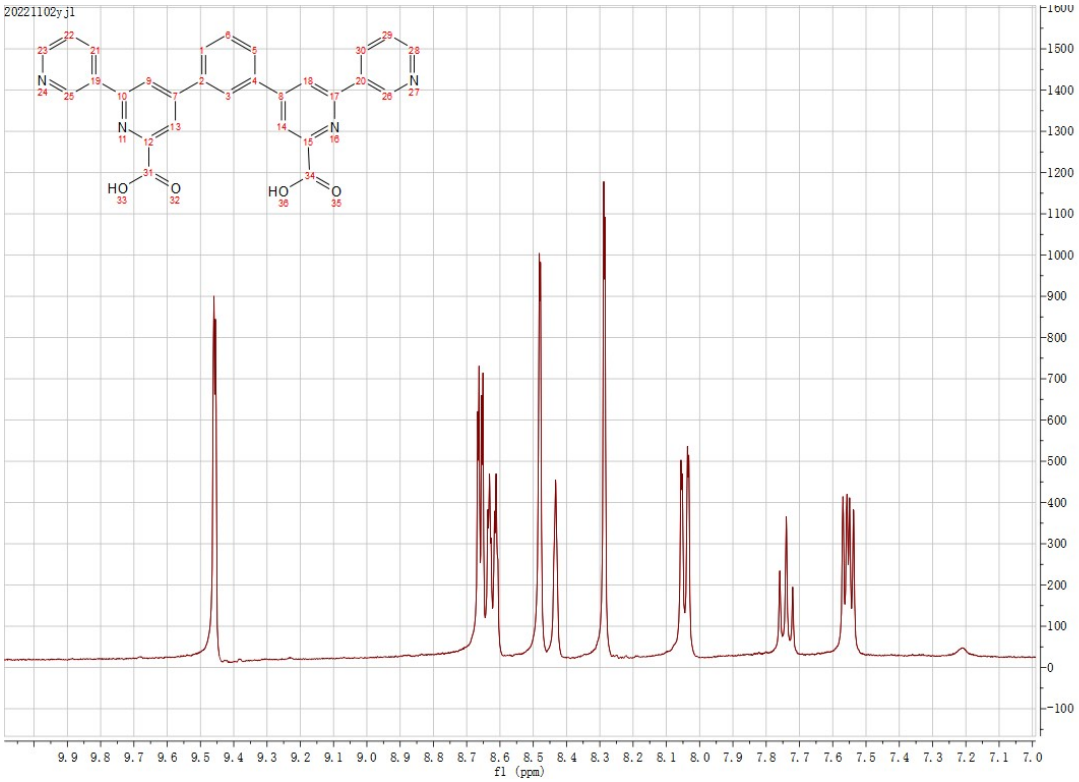

Fig. S1 ^1H NMR (400 MHz, dmso-d_6) of H_2L1 ligand.

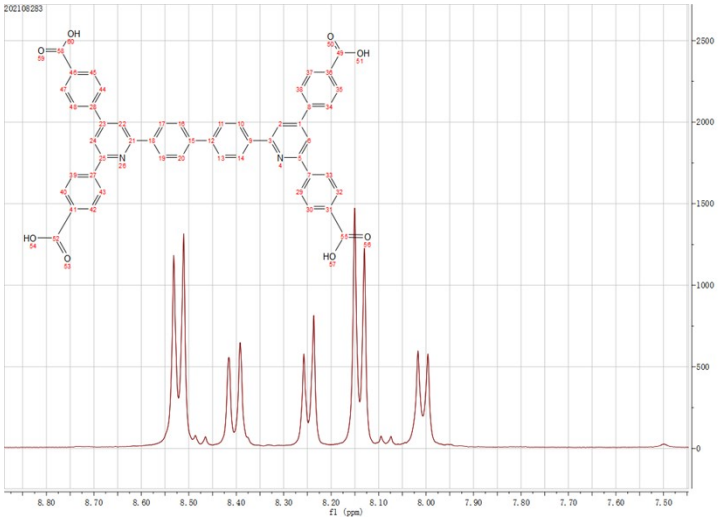

Fig. S2 ^{1}H NMR (400 MHz, dmso-d_6) of H_4L2 ligand.

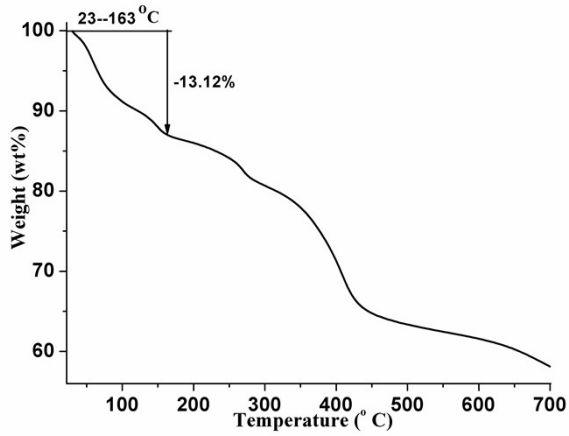

Fig. S3 TGA curve of **1**.

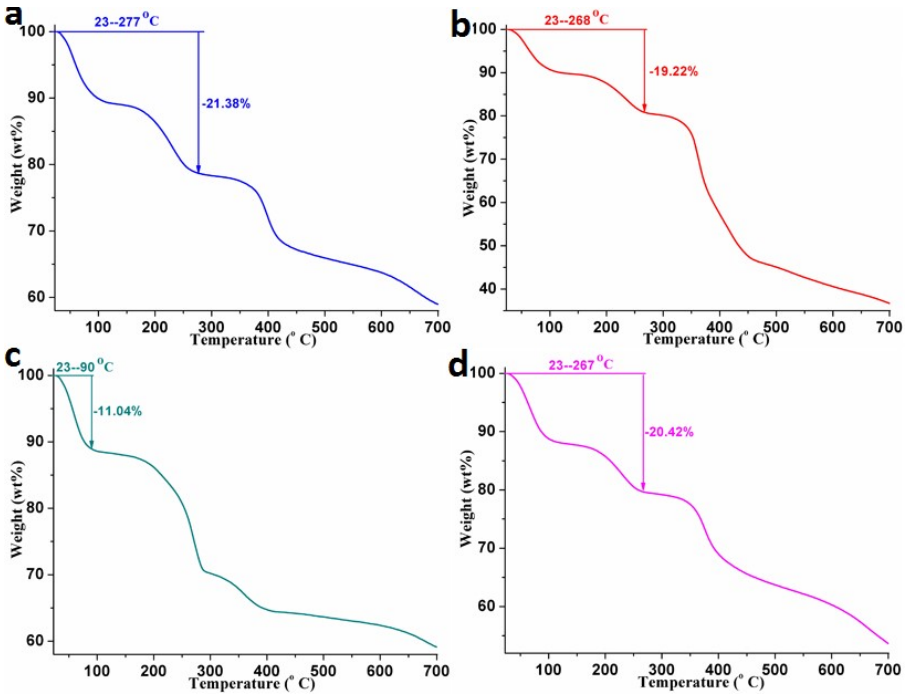

Fig. S4 TGA curves of **2** (a), **3** (b), **4** (c) and **5** (d).

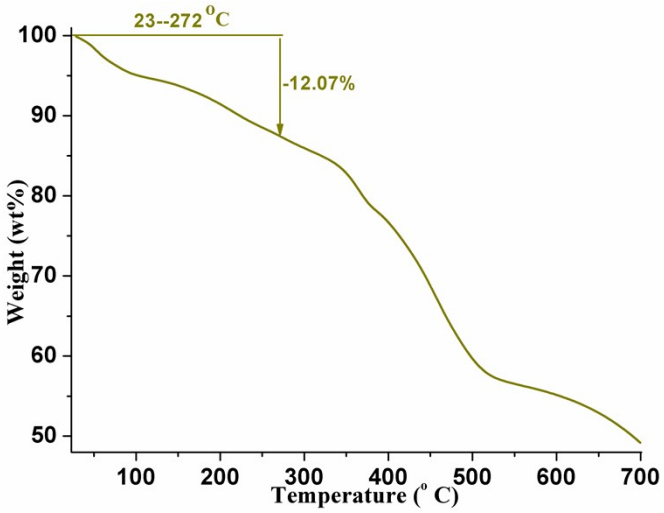

Fig. S5 TGA curve of **6**.

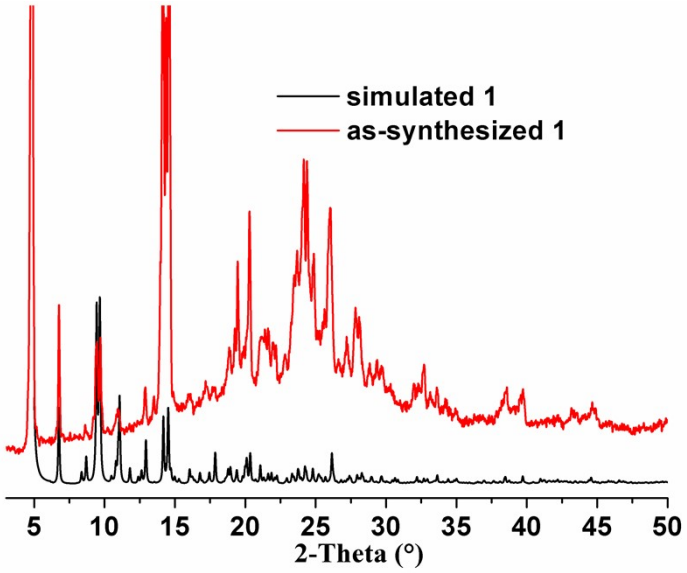

Fig. S6 Powder XRD profiles of **1**.

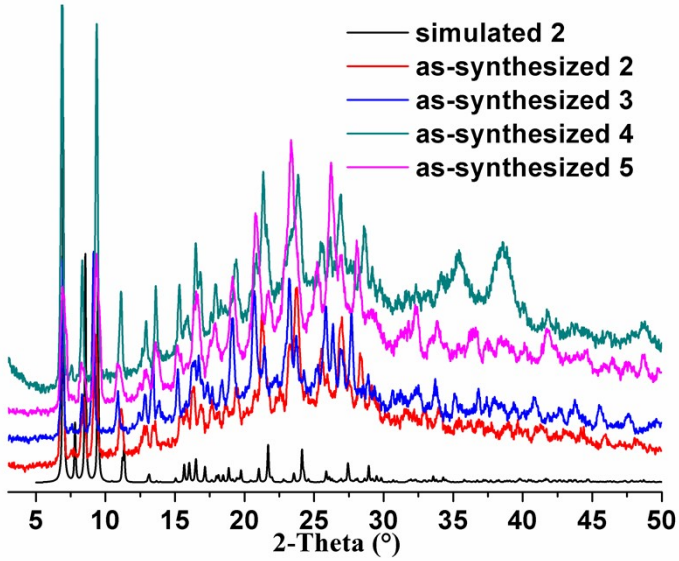

Fig. S7 Powder XRD profiles of **2**–**5**.

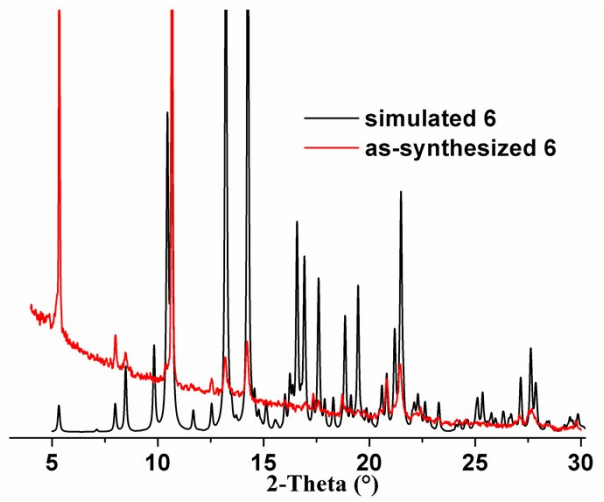

Fig. S8 Powder XRD profiles of **6**.

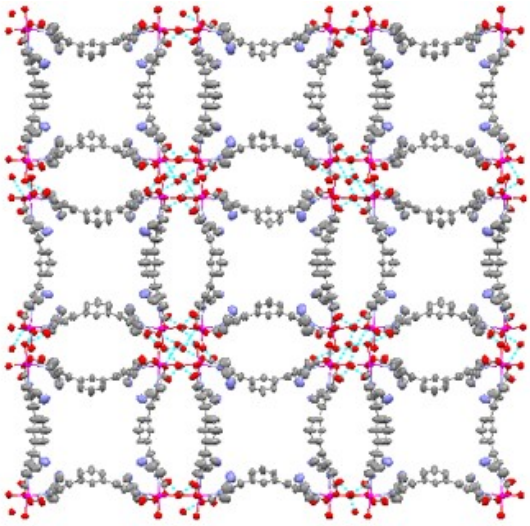

Fig. S9 2D supramolecular network of **1**.

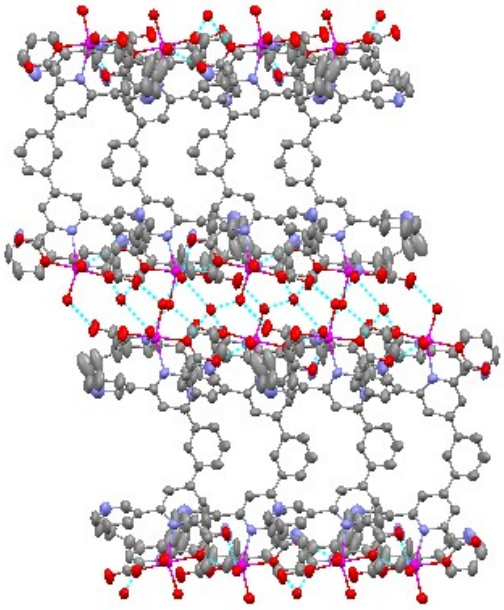

Fig. S10 The 3D supramolecular structure of **1** assembled by the antiparallel A-A packing mode.

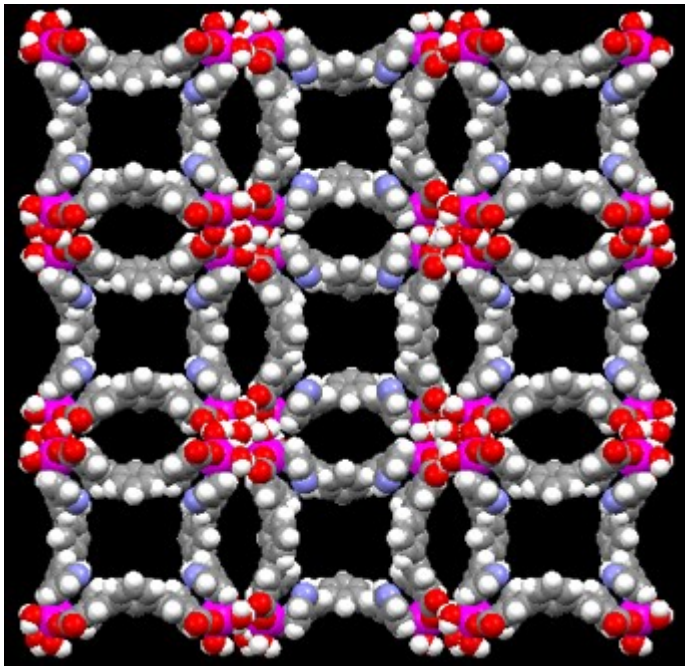

Fig. S11 Space-filling representation, showing guest-free channels including orthogon nanoscale channels in **1**.

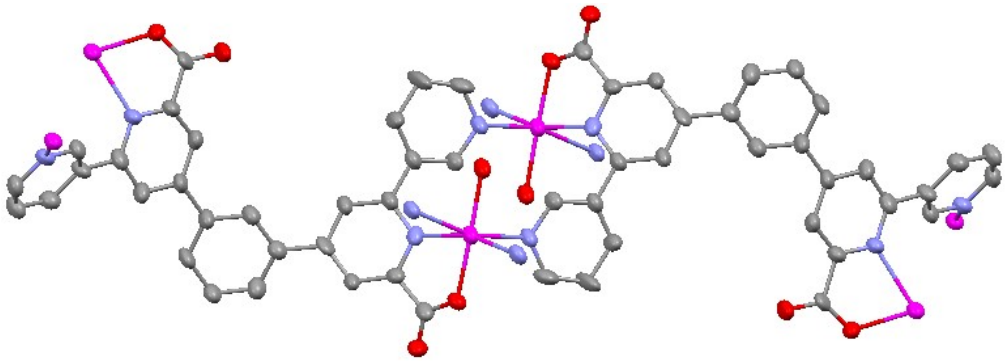

Fig. S12 The rhombus binuclear SBU in **2**.

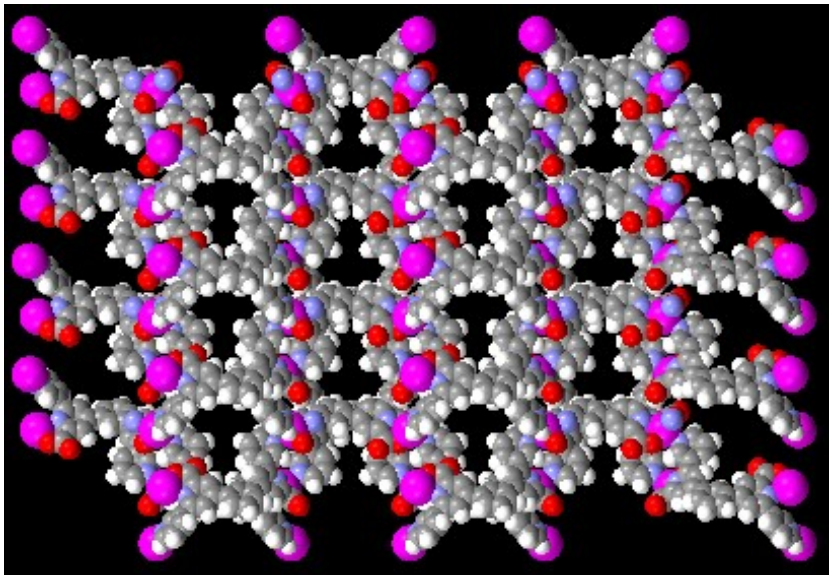

Fig. S13 Space-filling representation, showing guest-free "T-shaped" channels in **2**.

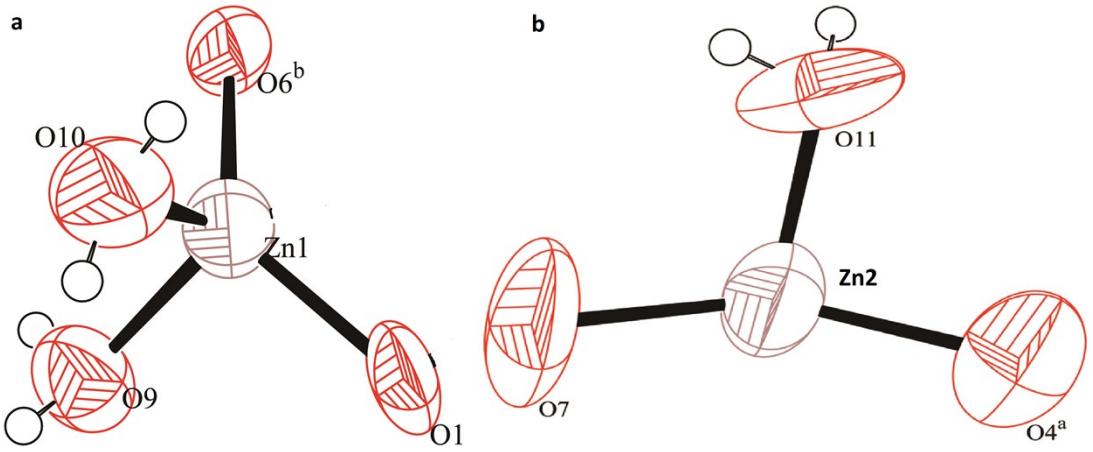

Fig. S14 ORTEP diagram showing coordination environment of Zn1 (a) and Zn2 (b) centers in **6** by thermal vibration ellipsoids with a 50% probability level. Symmetry code: a= -x, y+1/2, -z+1/2, b= -x, -y, -z.

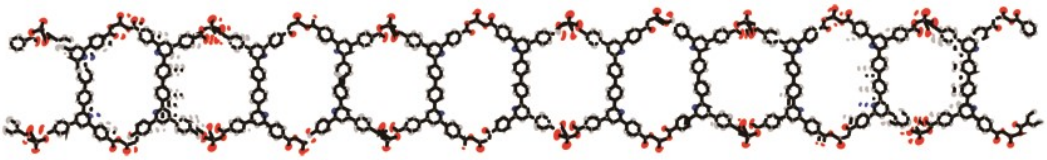

Fig. S15 Open channels in **6** along the *b* axis.

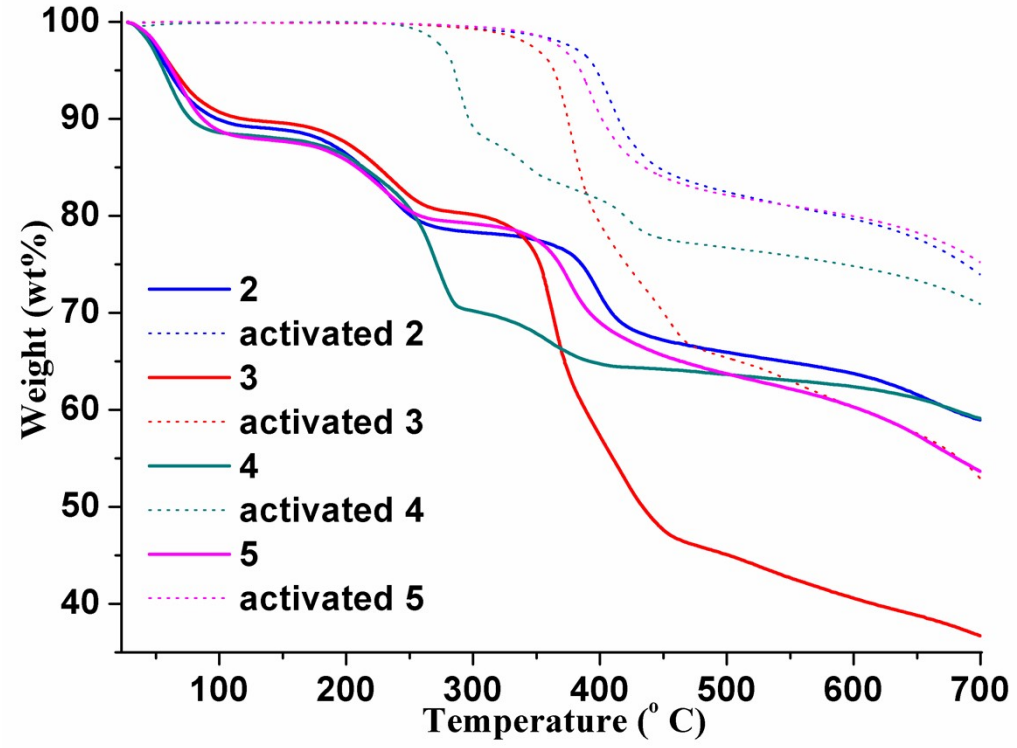

Fig. S16 TGA curves of **2**−**5** (solid lines), and activated **2**−**5** (dot lines).

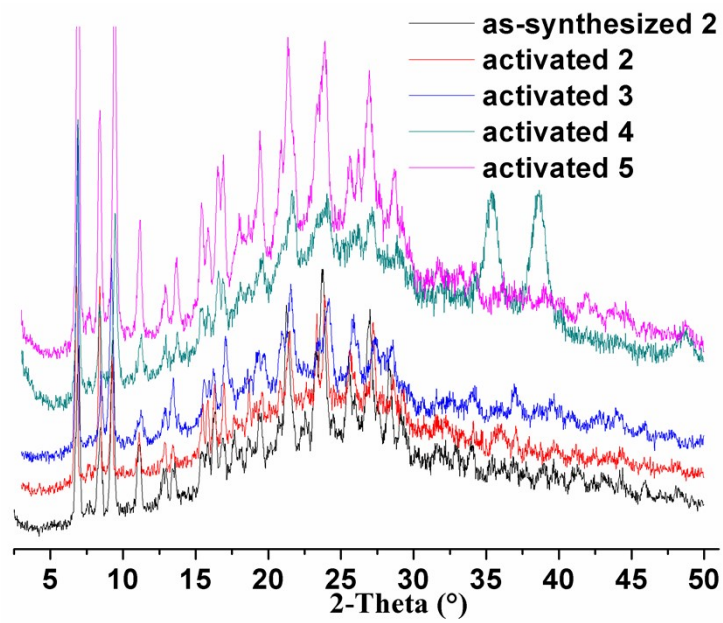

Fig. S17 Powder XRD profiles of as-synthesized **2** and activated **2**–**5**.

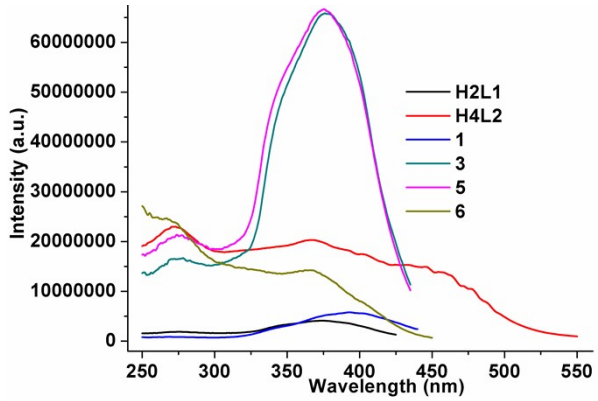

Fig. S18 Solid-state excitation spectra of H_2L1 and H_4L2 ligand and **1**, **3**, **5** and **6**.

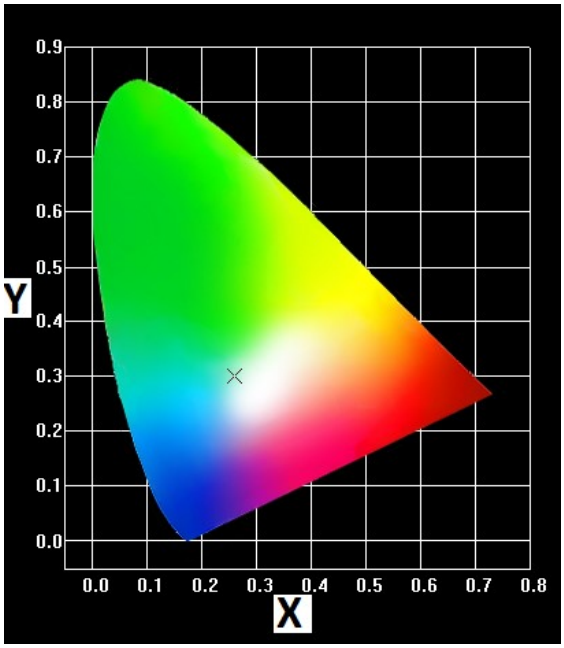

Fig. S19 CIE chromaticity diagram for **1** upon excitation at 365 nm.

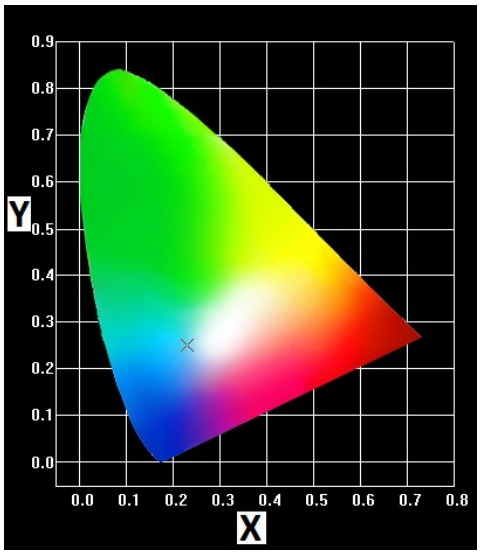

Fig. S20 CIE chromaticity diagram for **3** upon excitation at 365 nm.

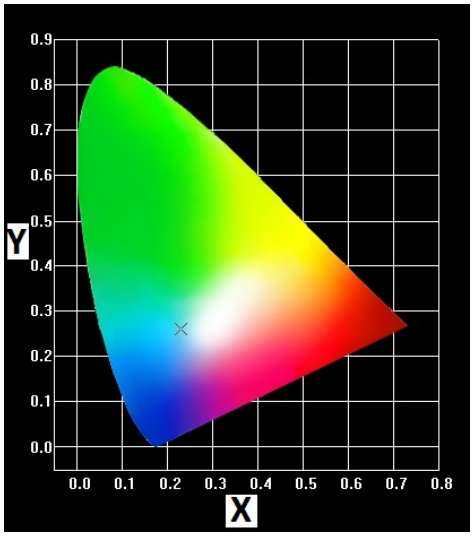

Fig. S21 CIE chromaticity diagram for **5** upon excitation at 365 nm.

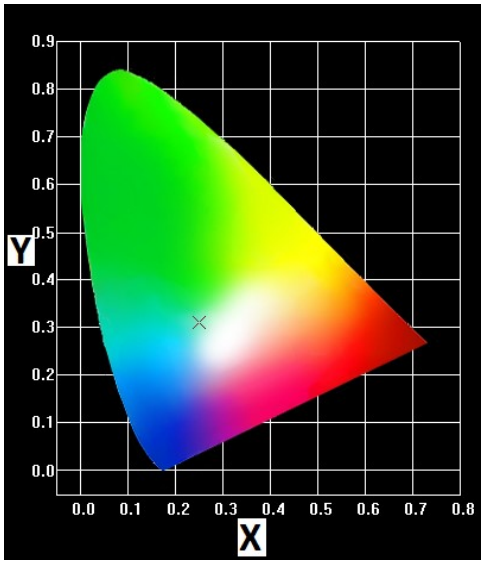

Fig. S22 CIE chromaticity diagram for activated **3** upon excitation at 365 nm.

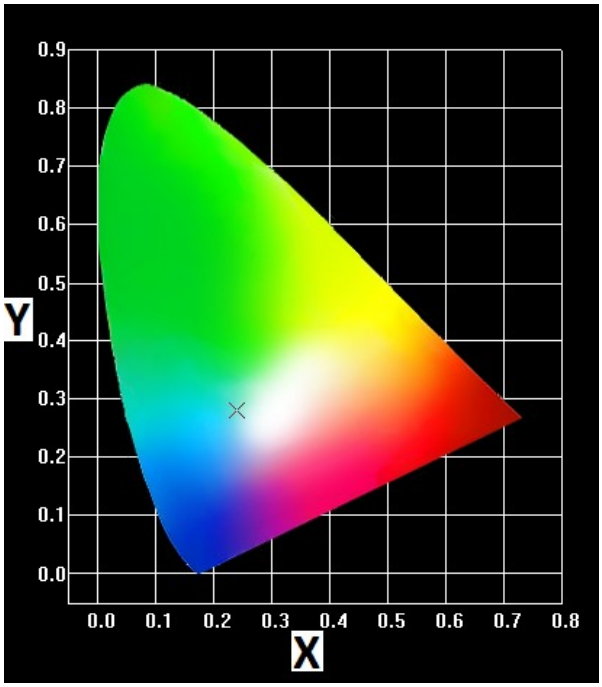

Fig. S23 CIE chromaticity diagram for activated **5** upon excitation at 365 nm.

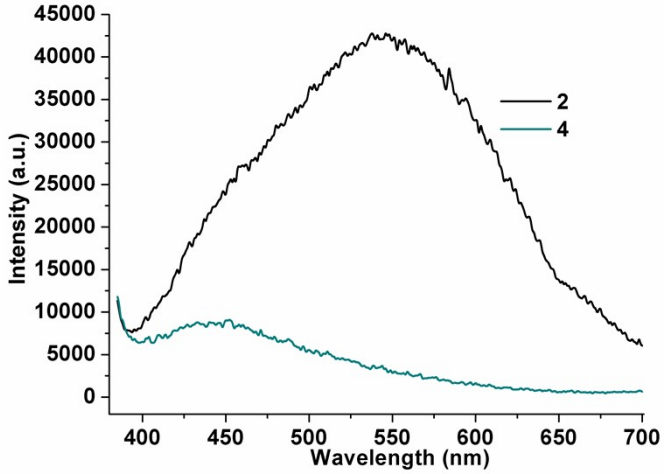

Fig. S24 PL spectra of 3D MOFs **2** and **4**.

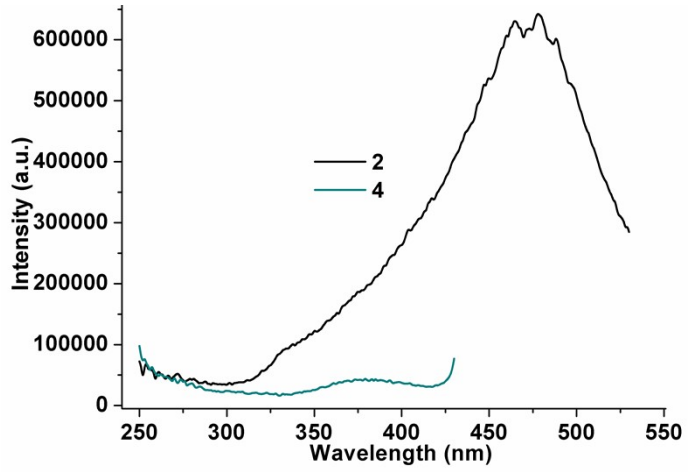

Fig. S25 Solid-state excitation spectra of 3D MOFs **2** and **4**.

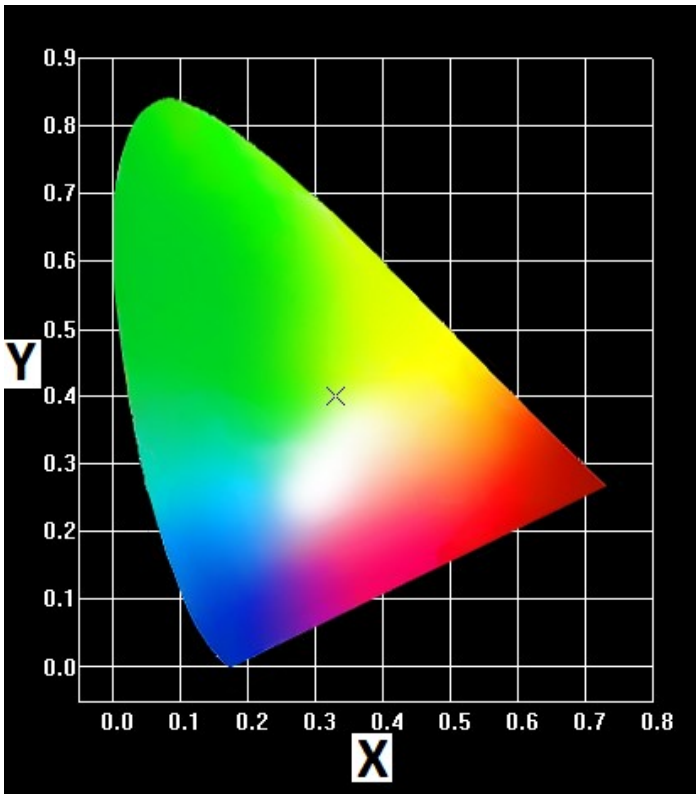

Fig. S26 CIE chromaticity diagram for **6** upon excitation at 365 nm.